Research Article

Kamran Behdinan, Rasool Moradi-Dastjerdi, Babak Safaei, Zhaoye Qin*, Fulei Chu, and David Hui

Graphene and CNT impact on heat transfer response of nanocomposite cylinders

https://doi.org/10.1515/ntrev-2020-0004
Received Dec 15, 2019; accepted Dec 28, 2019

Abstract: Reinforcing polymers with nanofillers is an advanced approach to improve and manage the thermal behaviors of polymeric nanocomposite materials. Among the proposed nanofillers, graphene and carbon nanotube (CNT) with superior thermal conductivity are two advanced nanofillers, which have extensively been utilized to enhance the heat transfer responses of host polymeric materials. In this work, the impacts of randomly oriented graphene and CNT to steady state and transient heat transfer behaviors of functionally graded (FG) nanocomposite cylinders have been investigated using an axisymmetric model. Nanocomposite cylinders have been assumed to be under heat fluxes, heat convections or temperatures as different types of thermal boundary conditions. The thermal properties of the resulted nanocomposite materials are estimated by micromechanical model. Moreover, the governing thermal equations of axisymmetric cylinders have been analyzed using a highly consistent and reliable developed mesh-free method. This numerical method predicts temperature fields via MLS shape functions and imposes essential boundary conditions with transformation approach. The effects of nanofiller content and distribution as well as thermal boundary conditions on the heat transfer responses of nanocomposite cylinders are studied. The results indicated that the use of nanofiller resulted in shorter stationary times and higher temperature gradients in FG nanocomposite cylinders. Moreover, the use of graphene in nanocomposites had stronger impact on thermal response than CNT.

Keywords: Heat transfer response; Transient and steady state; Graphene and CNT; Axisymmetric nanocomposites cylinders; Mesh-free method

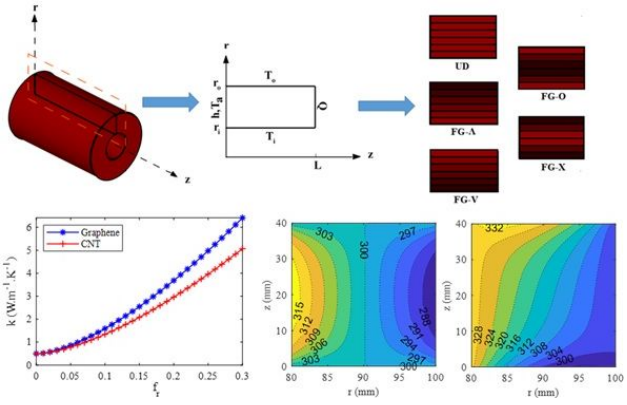

Graphical abstract

1 Introduction

In recent decades, the use of nanocomposite structures has been growing rapidly and has attracted much attention from scientific research communities [1, 2]. Among the utilized nanofillers, CNT and graphene have become very popular due to their unique thermo-mechanical properties. Specifically, values of up to 3000 W/m·K [3, 4] and 5300 W/m·K [5] for the thermal conductivities of CNT and graphene have been reported, respectively. Because of such extraordinary thermal behavior, these two nanofiller

*Corresponding Author: Zhaoye Qin: Department of Mechanical Engineering, Tsinghua University, Beijing, 100084, China; Email: qinzy@mail.tsinghua.edu.cn
Kamran Behdinan: Advanced Research Laboratory for Multifunctional Lightweight Structures (ARL-MLS), Department of Mechanical & Industrial Engineering, University of Toronto, Toronto, Canada; Email: behdinan@mie.utoronto.ca
Rasool Moradi-Dastjerdi: Advanced Research Laboratory for Multifunctional Lightweight Structures (ARL-MLS), Department of Mechanical & Industrial Engineering, University of Toronto, Toronto, Canada; Email: moradi@mie.utoronto.ca
Babak Safaei: Department of Mechanical Engineering, Eastern Mediterranean University, G. Magosa, TRNC Mersin 10, Turkey; Email: babak.safaei@emu.edu.tr
Fulei Chu: Department of Mechanical Engineering, Tsinghua University, Beijing, 100084, China; Email: chufl@mail.tsinghua.edu.cn
David Hui: Department of Mechanical Engineering, University of New Orleans, New Orleans, LA 70148, United States of America; Email: dhui@uno.edu

are excellent candidates to improve thermal conductivity of polymeric nanocomposite materials. On the other hand, it is well established that the FG dispersion of nanofiller in nanocomposite materials results in more manageable thermal-mechanical responses of nanocomposite structures [6–10].

Since thermal analysis is very critical in engineering structures, many researchers have investigated the thermal conductivity of nanocomposite materials. These materials and structures generate one of the hot topics of research in several emerging technologies and, therefore, they are being extensively investigated by researchers because of considerably improved their thermo-mechanical behaviors [11, 12]. Several parameters including nanofiller size, volume fraction, aspect ratio, thermal conductivity and intersection thermal resistance as well as temperature and nanofiller-matrix interface stickiness have influence on the effective thermal conductivity of nanocomposites. Highly conductive fillers, like metallic or carbon-based materials, can be added into nanocomposite cylinders to improve their thermal conductivity [13, 14]. Dispersion/ aggregation state and filler shape are the critical factors influencing the thermal conductivity of nanofluids and solid composites. Regarding nanofillers, the resistance of thermal interfacial is another critical factor affecting thermal transport. Researchers believe that the main factor limiting the thermal performance of suspensions and CNT composites is interfacial thermal resistance [15–17]. Gu *et al.* [18] performed some tests and proved that the use of 21.4% graphene platelets in a type of polyethylene (PE) called ultra-high molecular weight polyethylene (UHMWPE) increased the thermal conductivity of host material by up to around nine times the original UHMWPE matrix. Zabihi *et al.* [19] studied the effects of different types of defects on the effective thermal conductivity of nanocomposite materials reinforced with defected CNT, graphene and hybrid CNT/graphene fillers. Moheimani *et al.* [20] also conducted extensive research on the development of a closed-form unit cell micromechanical model for determining the effective thermal conductivities of unidirectional CNTs reinforced polymer nanocomposites.

Nanocomposite materials reinforced with CNT or graphene have been extensively utilized in different shell and plate structures in order to analyze their structural thermo-mechanical responses by many researchers in recent years. Qin *et al.* [21] proposed unified solution for laminated FG shallow shells reinforced by graphene with general boundary conditions; upon which free vibration of FG cylindrical shells and plates reinforced by CNTs and graphene with both classic and non-classic boundary conditions were investigated [22, 23]. Shokri-Oojghaz [24] studied the effect of reinforcing with aggregated CNT on the stress distributions of nanocomposite sandwich cylinders based on finite element method. Temperature effect on the static and dynamic responses of nanocomposite cylinders reinforced with wavy CNT were studied by Moradi-Dastjerdi *et al.* [25–27]. Safaei *et al.* [28] analyzed the free vibration of nanocomposite plates with CNTs embedded in amorphous polyethylene. They used the rules of mixture according to different plate model theories to find the fundamental frequencies of nanocomposite plates. The macro-mechanical characteristics of nanocomposites are influenced by CNT and graphene volume fraction and microstructure. Safaei *et al.* [29, 30] examined the thermal and mechanical behaviors of lightweight polymeric nanocomposite porous sandwich plates resting on two-parameter elastic foundation. Damadam *et al.* [31] found that the increase of non-dimensional temperature led to ratcheting in plastic strain in subsequent cycles. Furthermore, they introduced Bree's Diagram to more effectively plot the material behavior of thick-walled cylinders under different loading conditions and were able to identify safe loading boundary for different temperatures and pressures. Jalali *et al.* [32] studied mechanical analysis of micro FG beams considering thermal conditions using a numerical method to see the effect of temperature change in natural frequencies of FG micro beams. The effects of thermal conductivity, temperature change, heat wave speed, heat flux, CNTs volume fraction and end support conditions on the nonlinear vibration of beam were discussed in detail by Pourasghar and Chen [33]. They also combined the applications of differential quadrature and Newton Raphson methods and used the developed method to solve the non-Fourier heat conduction equations to obtain temperature, displacement and stress in CNT reinforced, nanocomposite cylindrical panels [34]. Safaei *et al.* [35] investigated transient heat transfer and stress wave propagation in polymeric sandwich plates with two nanocomposite face sheets were made of clusters of CNTs embedded in a polymeric matrix. Zargar *et al.* [36] investigated thermal response of porous circular fins using numerical/analytical methods to see the effect of different geometry and nondimensional parameters in this problem. Moradi-Dastjerdi and Behdinan [37] studied the effect of graphene on the static and free vibration responses of nanocomposite cylinders subjected to thermal gradient load. Moreover, steady state and transient heat transfer responses of CNT-reinforced cylinders were performed in [38].

As mentioned in the above literature review, the effect of graphene or CNT on the thermal conductivity of polymeric nanocomposite materials has widely been investi-

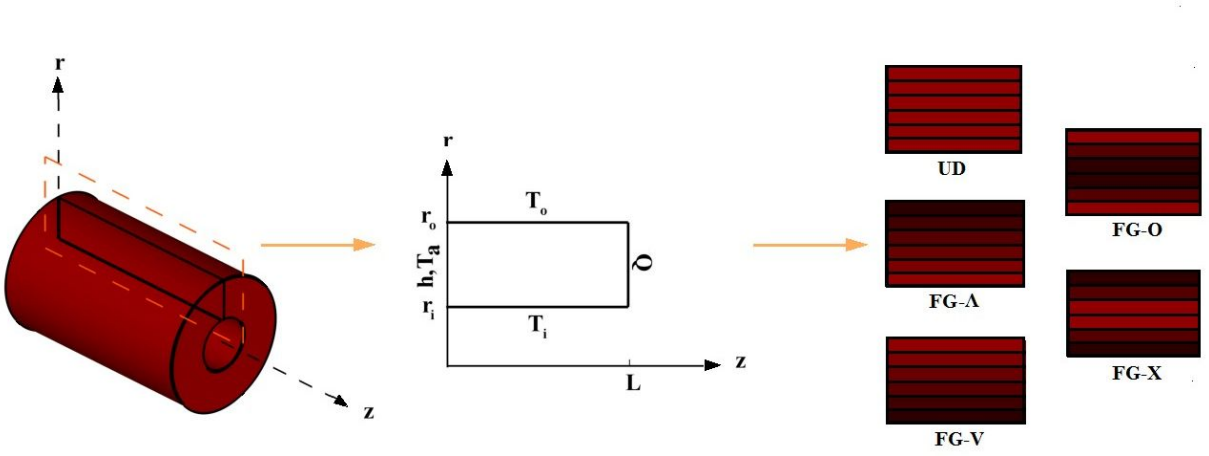

Figure 1: Axisymmetric nanocomposite cylinders with UD and FG distribution patterns of nanofillers subjected to various thermal boundary conditions

gated in literature. However, the impacts of these outstanding nanofillers on the heat transfer responses of axisymmetric cylinders have not fully been considered yet. Therefore, in this work, we have tried to address this shortcoming by the investigation and comparison of the heat transfer responses of FG axisymmetric cylinders reinforced with randomly oriented graphene or CNT. To do so, nanocomposite cylinders subjected to different thermal boundary conditions were considered. It should be noted that the thermal conductivities of nanocomposite materials were estimated through an accurate micromechanical model. Moreover, governing thermal equation was derived using a developed mesh-free method which included MLS shape function and transformation approach. Using the developed methods, the effects of nanofiller content and distribution as well as thermal boundary conditions on the heat transfer responses of FG nanocomposite cylinders were presented.

2 Modeling of nanocomposite cylinders

As mentioned earlier, randomly orientated graphene and CNT were selected as nanoscale reinforcements of nanocomposite cylinders with length L, inner radius r_i, and outer radius r_o, as illustrated in Figure 1. The boundaries of nanocomposite cylinders were assumed to be subjected to a constant temperature T, heat flux Q or thermal convection with ambient temperature T_a and convective heat transfer coefficient h. All the thermal boundary conditions are also assumed to be uniform on their surfaces. It should be noted that boundary conditions and structure are axisymmetric, therefore, three-dimensional analysis of such structures can be reduced to a two-dimensional analysis without losing the accuracy of in results.

2.1 Dispersion of nanofillers

With the aim of optimizing the amount of utilized nanofillers to provide the best design, the concept of FGMs was employed in this work. Therefore, four linear FG profiles were selected for the dispersions of nanofillers along the radial direction of cylinders. In addition, a nanocomposite cylinder with uniform dispersion (UD) profile was considered to compare its steady state and transient thermal responses with FG nanocomposite cylinders.

According to the dispersions of nanofillers, the four FG types of dispersion were labeled as V, ∧, X and O. The schematic FG distributions of nanofillers are shown in Figure 2. The variations of the volume fraction of nanofillers $f_r(r)$ was also described as the following equations [37]:

$$\text{FG}-\text{V}: \; f_r(r) = \Delta f_r(r - r_i)/h + f_r^{\min} \tag{1a}$$

$$\text{FG}-\wedge: \; f_r(r) = \Delta f_r(r_o - r)/h + f_r^{\min} \tag{1b}$$

$$\text{FG}-\text{X}: \; f_r(r) = 2\Delta f_r|r - r_m|/h + f_r^{\min} \tag{1c}$$

$$\text{FG}-\text{O}: \; f_r(r) = f_r^{\max} - 2\Delta f_r|r - r_m|/h \tag{1d}$$

$$\text{UD}: \; f_r(r) = \left(f_r^{\max} + f_r^{\min}\right)/2 \tag{1e}$$

where r_m is the mid radius of cylinder. Moreover, the difference between the maximum $f_r^{\max}$ and minimum $f_r^{\min}$ values of nanofiller volume fractions is shown with Δf_r.

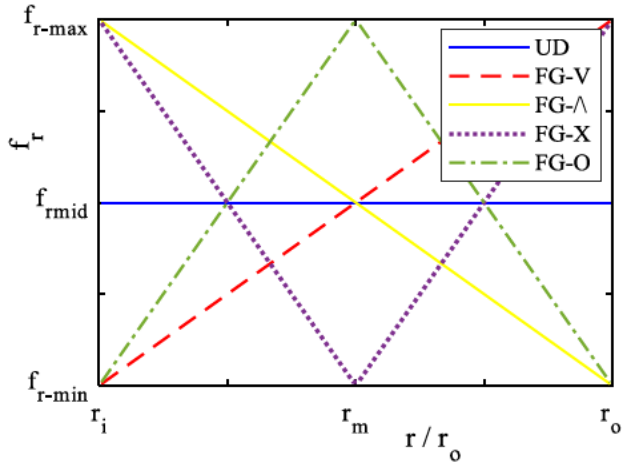

Figure 2: Nanofiller distributions along the radial direction according to the proposed profiles

2.2 Thermal properties

The thermal conductivity of polymeric nanocomposite materials reinforced with graphene or CNT can be estimated by employing a micromechanical model developed in [39] and modified in [19, 40]. This method was based on the volume fractions f_r, thermal conductivity k^r and aspect ratio p of nanofillers. According to this method, the thermal conductivities of nanocomposite materials reinforced with graphene or CNT was estimated as follow [19, 40]:

$$\frac{k^e(r)}{k^m} = 1 + \frac{F_c}{H + \left(\frac{K^f}{k^m} - 1\right)} \tag{2}$$

where

$$H = \frac{1}{p^2 - 1}\left[\frac{p}{\sqrt{p^2 - 1}} \ln\left(p + \sqrt{p^2 - 1}\right) - 1\right] \tag{3}$$

$$\text{For graphene}: \; F_c = \frac{2}{3}\left(f_r - \frac{1}{p}\right)^{1.5}, \qquad K^f = \frac{k^r}{1 + \frac{2R_k k^r}{l}} \tag{4}$$

$$\text{For CNT}: \; F_c = \frac{1}{3}\left(f_r - \frac{0.6}{p}\right)^{1.5}, \quad K^f = \frac{k^r}{1 + \frac{R_k k^r}{l}} \tag{5}$$

where k^m is the thermal conductivity of polymeric matrix and l and R_k are nanofiller length and thermal resistance between the interfaces of nanofiller-nanofiller and nanofiller-polymeric, respectively. It should be noted that the estimation of k through this approach was already verified by experimental results of graphene [18] and CNT-reinforced [41] polymers.

Furthermore, the mass density ρ and specific heat conduction c_p of the resulted nanocomposite materials were roughly calculated as follow:

$$c_p = f_r c_p^r + f_m c_p^m, \quad \rho = f_r \rho^r + f_m \rho^m \tag{6}$$

where the superscripts of r and m indicate nanofiller and matrix, respectively, and matrix volume fraction is shown by $f_m = 1 - f_r$.

3 Meshless formulations

The governing equation for transient heat conduction in an FG axisymmetric cylinder was stated as [38, 42]:

$$\frac{1}{r}\left[k(r)\frac{\partial}{\partial r}\left(r\frac{\partial T(r,z)}{\partial r}\right)\right] + k(r)\frac{\partial^2 T(r,z)}{\partial z^2} = \rho(r)c_p(r)\frac{\partial T(r,z)}{\partial t} \tag{7}$$

where t is time and $T(r,z)$ is temperature at point $\mathbf{X} = \mathbf{X}_i(r,z)$. The initial and boundary conditions were also defined as:

$$\begin{aligned} T(r,z) &= T^0 \text{ at } t = t_0 \\ T &= T_1 \text{ on } \Gamma_1, \quad Q = Q_2 \text{ on } \Gamma_2, \\ h &= h_a \text{ and } T_a \text{ on } \Gamma_3 \end{aligned} \tag{8}$$

where Γ shows boundaries including inner, outer, upper and lower surfaces of axisymmetric cylinders.

To analyze the thermal conduction of the considered nanocomposite cylinders, the weak form of Eq. (7) was treated through the standard form of Galerkin method. Developing a mesh-free method based on moving least square (MLS) shape functions $\mathbf{\Phi}$, the vector of generalized values of temperature field $\hat{\mathbf{T}}$ were estimated as [43]:

$$\hat{\mathbf{T}} = \sum_{i=1}^{n} \Phi_i T_i = \mathbf{\Phi}\,\mathbf{T} \tag{9}$$

where

$$\begin{aligned} &\mathbf{T} = [T_1, T_2, .., T_n]^T, \quad \hat{\mathbf{T}} = \left[\hat{T}_1, \hat{T}_2, .., \hat{T}_n\right]^T, \\ &\mathbf{\Phi} = [\Phi_1, \Phi_2, .., \Phi_n]^T \end{aligned} \tag{10}$$

where n is node number located inside the support domain of the defined shape function. Moreover, MLS shape function at $\mathbf{X} = \mathbf{X}_i(r,z)$ was described as [43]:

$$\Phi_i(\mathbf{X}) = \underbrace{\mathbf{P^T}(\mathbf{X})\left[\mathbf{M}(\mathbf{X})\right]^{-1} w(\mathbf{X} - \mathbf{X}_i)\mathbf{P}(\mathbf{X}_i)}_{(1\times 1)} \tag{11}$$

where $\mathbf{P}$, w and $\mathbf{M}$ are base vector, cubic Spline weight function and moment matrix, respectively. In axisymmetric condition, $\mathbf{P}$ and $\mathbf{M}$ were determined as:

$$\mathbf{P}(\mathbf{X}) = [1, r, z]^T, \tag{12}$$
$$\mathbf{M}(\mathbf{X}) = \left[\sum_{i=1}^{n} w(\mathbf{X} - \mathbf{X}_i)\mathbf{P}(\mathbf{X}_i)\mathbf{P}^{\mathbf{T}}(\mathbf{X}_i)\right]$$

The submission of approximated temperature field Eq. (9) in the weak form of governing thermal equation Eq. (7) was resulted in following discrete mesh-free form [38]:

$$\mathbf{C}\frac{d\hat{\mathbf{T}}}{dt} + \mathbf{K}_T\hat{\mathbf{T}} - \int_{\Gamma} \mathbf{\Phi}^T(-M_T\mathbf{T} + S)d\Gamma = 0 \tag{13}$$

where $M_T = 0$ and $S = Q$ for boundaries subjected to thermal flux, and $M_T = h$ and $S = hT_a$ for boundaries under convection environment. By applying such boundary conditions, Eq. (13) was rearranged as:

$$\mathbf{C}\frac{d\hat{\mathbf{T}}}{dt} + \mathbf{K}_T\hat{\mathbf{T}} + \mathbf{K}_M\hat{\mathbf{T}} = \mathbf{Q} \tag{14}$$

where

$$\mathbf{K}_T = \int_{\Omega} \mathbf{B}^T\mathbf{D}\mathbf{B}\,dv, \quad \mathbf{K}_M = \int_{\Gamma} M_T\mathbf{\Phi}^T\mathbf{\Phi}dv, \tag{15}$$
$$\mathbf{C} = \int_{\Omega} (\rho c_p)\mathbf{\Phi}^T\mathbf{\Phi}dv, \quad \mathbf{Q} = \int_{\Gamma} Q\mathbf{\Phi}^T ds$$

in which

$$\mathbf{B} = \begin{bmatrix} \frac{\partial \Phi_1}{\partial r} & \frac{\partial \Phi_2}{\partial r} & \cdots & \frac{\partial \Phi_n}{\partial r} \\ \frac{\partial \Phi_1}{\partial z} & \frac{\partial \Phi_2}{\partial z} & \cdots & \frac{\partial \Phi_n}{\partial z} \end{bmatrix}, \quad \mathbf{D} = k(r)\begin{bmatrix} 1 & 0 \\ 0 & 1 \end{bmatrix} \tag{16}$$

Before the solution of Eq. (14), essential boundary conditions had to be applied to this equation. However, such condition could not directly be imposed because Eq. (14) was based on the generalized values of temperature field. This extra process was due to the shortcoming of MLS shape functions in the satisfaction of Kronecker delta property. To overcome this problem, a transformation matrix $\mathbf{R}$ was employed to modify $\hat{\mathbf{T}}$ as follows [38]:

$$\overline{\mathbf{T}} = \mathbf{R}\hat{\mathbf{T}} \tag{17}$$

where $\overline{\mathbf{T}}$ is the vector of calculated nodal values of temperature field. The transformation matrix was defined as:

$$\mathbf{R} = \begin{bmatrix} \Phi_1(\mathbf{X}_1) & \Phi_2(\mathbf{X}_1) & . & . & \Phi_n(\mathbf{X}_1) \\ \Phi_1(\mathbf{X}_2) & \Phi_2(\mathbf{X}_2) & & & \Phi_n(\mathbf{X}_2) \\ . & . & . & . & . \\ . & . & . & . & . \\ \Phi_1(\mathbf{X}_n) & \Phi_2(\mathbf{X}_n) & . & . & \Phi_n(\mathbf{X}_n) \end{bmatrix} \tag{18}$$

The substitution of Eq. (17) in Eq. (14) gave:

$$\hat{\mathbf{C}}\frac{d\overline{\mathbf{T}}}{dt} + \hat{\mathbf{K}}_T\overline{\mathbf{T}} + \hat{\mathbf{K}}_M\overline{\mathbf{T}} = \hat{\mathbf{Q}} \tag{19}$$

where,

$$\hat{\mathbf{C}} = \mathbf{R}^{-\mathbf{T}} \cdot \mathbf{C} \cdot \mathbf{R}^{-\mathbf{1}}, \quad \hat{\mathbf{q}} = \mathbf{T}^{-\mathbf{T}} \cdot \mathbf{q} \tag{20}$$
$$\hat{\mathbf{K}}_T = \mathbf{R}^{-\mathbf{T}} \cdot \mathbf{K}_T \cdot \mathbf{R}^{-\mathbf{1}}, \quad \hat{\mathbf{K}}_M = \mathbf{R}^{-\mathbf{T}} \cdot \mathbf{K}_M \cdot \mathbf{R}^{-\mathbf{1}}$$

The essential boundary conditions be applied in Eq. (19) as easy as FEM.

4 Results and discussions

Steady state and transient heat transfer responses of the considered FG nanocomposite cylinders are presented in this section. Nanocomposite materials were made of a mixture of graphene or CNT as reinforcement part embedded in polyethylene as polymeric matrix. The properties of the materials employed in the simulations were [18, 19, 41]:

$$\textbf{PE}: k^m = 0.5\ W/m{\cdot}K, \quad c_p^m = 1466\ j/Kg{\cdot}K,$$
$$\rho^m = 1150\,Kg/m^3$$
$$\textbf{Graphene}: k^r = 3000\ W/m{\cdot}K, \quad c_p^r = 700\ j/Kg{\cdot}K,$$
$$\rho^r = 4118\,Kg/m^3, \quad l = 40\ \mu m,$$
$$p = 250, \quad R_k = 3.5 \times 10^{-9}$$
$$\textbf{CNT}: k^r = 3000\ W/m{\cdot}K, \quad c_p^r = 700\ j/Kg{\cdot}K,$$
$$\rho^r = 1400\,Kg/m^3, \quad l = 0.445\ \mu m,$$
$$p = 148,$$

According to Eq. (2), Figure 3 shows the variations of the thermal conductivities of CNT and graphene-reinforced nanocomposite materials as a function of

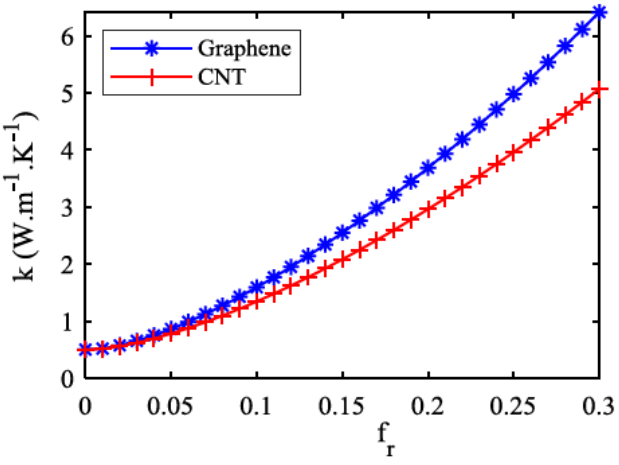

Figure 3: Thermal conductivities of graphene/PE and CNT/PE versus the volume fraction of nanofillers

nanofiller volume fraction. This figure shows that by the increase of nanofiller content, the thermal conductivities of both nanocomposites are significantly improved. The comparison between CNT and graphene shows that, graphene/PE nanocomposite enjoys higher thermal conductivity than CNT/PE nanocomposite because of graphene shape and PE-graphene thermal resistance R_k.

4.1 Validation study

Here, we examine the accuracy of the proposed solution framework for steady state and transient heat transfer responses of axisymmetric cylinders. First, the steady state responses of an isotropic axisymmetric long cylinder with inner temperature T_i = 300 K and outer temperature T_o = 350 K has been investigated. Hetnarski and Eslami [42] presented the exact solution of such cylinders as the following equation:

$$T = \frac{T_i - T_o}{\ln(r_o - r_i)} \ln(r_o - r) + T_b \tag{21}$$

Figure 4 compares the temperature profiles along cylinder thickness obtained from our solution with exact results. An excellent agreement between the results can be observed in this figure which shows the accuracy of the proposed solution method.

In addition to steady state response, the accuracy of the proposed method has been examined for transient response of graphene and CNT reinforced nanocomposite cylinders. In this case, we tracked the transient solutions of temperature profiles until their steady state conditions were achieved and compared the final profile of each cylinder with their corresponding temperature profiles obtained from steady state solution. Hence, we considered cylinders at initial temperature T^0 = 300 K subjected to inner heat flux Q_i = 8 kW/m^2 and outer heat convection environment with h_o = 200 W/m^{2}K and T_{a-o} = 250 K when upper and lower faces of cylinders are thermally insulated i.e. Q_u = 0 and Q_d = 0. In these cylinders, the volume fractions of nanofillers are varied from $f_r^{\min}$ = 0 to $f_r^{\max}$ = 0.3 trough the thickness according to X profile when the dimensions are L = 0.04 m, r_o = 0.1 m and r_i = 0.08 m. Figure 5 shows that the transient responses of both cylinders are gradually converged to steady state temperature profiles. After 2500 seconds, perfect consistency between transient response and steady state solutions are observed for both cylinders.

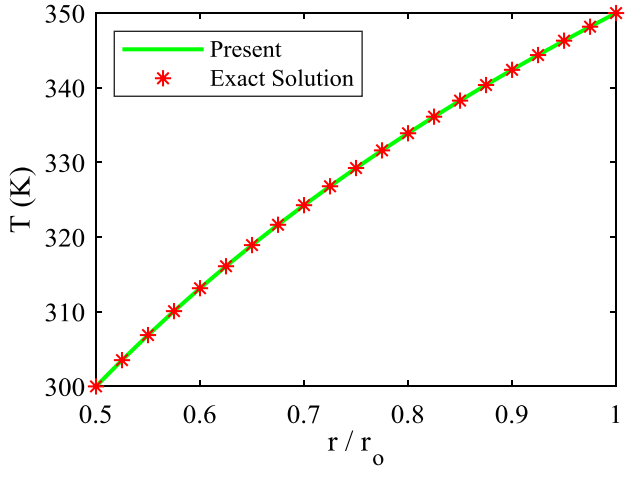

Figure 4: Comparison between temperature profiles along cylinder thickness obtained from the present method and exact solution [42]

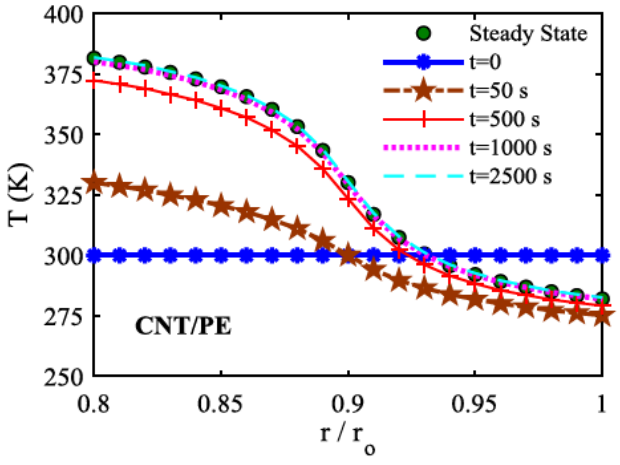

(a)

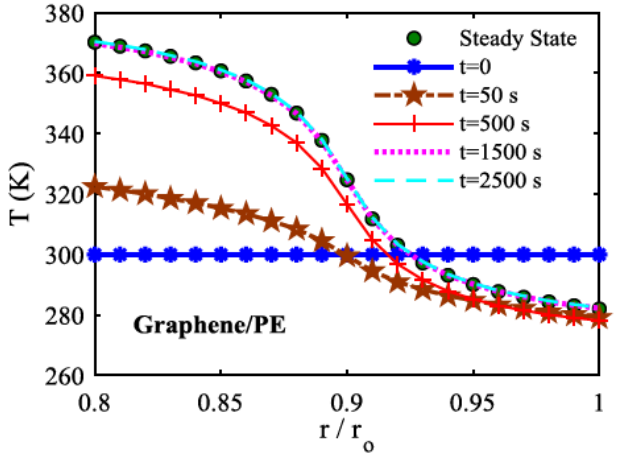

(b)

Figure 5: Steady state and transient temperature profiles along the thickness of (a) X-CNT/PE (b) X-graphene/PE cylinders at different times

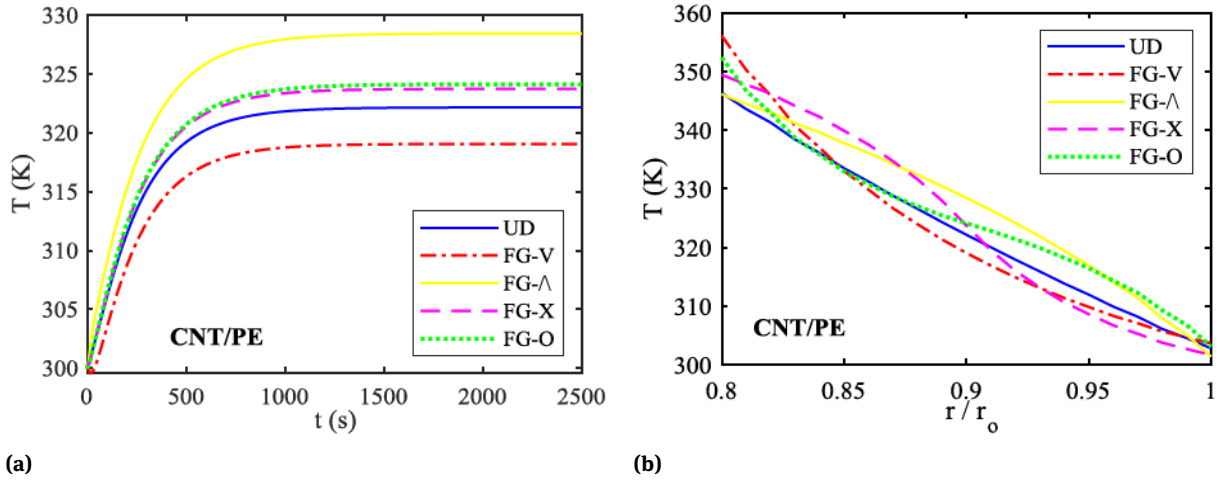

Figure 6: a) Temperature time histories of mid points b) Steady state temperature profiles at $z = L/2$ in FG and UD-CNT/PE cylinders

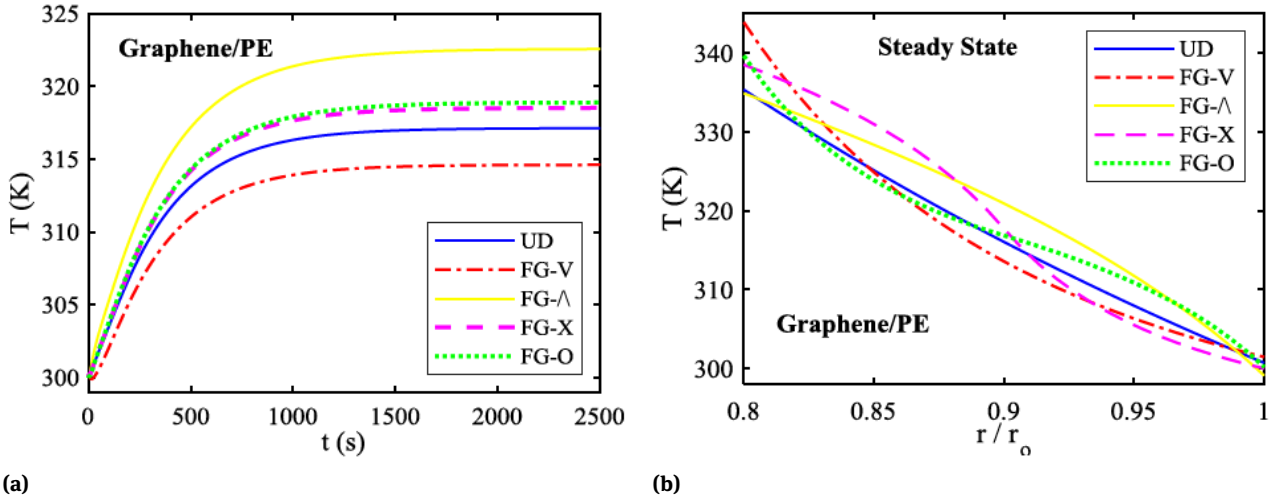

Figure 7: a) Temperature time histories of mid points b) Steady state temperature profiles at $z = L/2$ in FG and UD-graphene/PE cylinders

4.2 Heat transfer response

Once the developed mesh-free method was validated, the transient heat transfer of FG nanocomposite cylinders reinforced with graphene or CNT were investigated under a variety of boundary conditions. The effects of nanofiller distribution on temperature profile and the time required to reach steady state condition have been studied. Therefore, nanocomposite cylinders with $L = 0.04$ m, $r_i = 0.08$ m, $r_o = 0.1$ m, $f_r^{\min} = 0.1$, $f_r^{\max} = 0.3$ and $T^0 = 300$ K were considered. The inner and upper surfaces of cylinders are assumed under the heat fluxes of $Q_i = 8$ kW/m^2 and $Q_u = 4$ kW/m^2. In addition, the bottom and outer surfaces are in heat convection environments with $h_o = 100$ W/(m^{2}K), $h_d = 200$ W/(m^{2}K) and $T_{a-o} = T_{a-d} = 250$ K. Figure 6a shows temperature time histories of FG and UD-CNT reinforced nanocomposite cylinders at their mid points. Figure 6b also shows temperature distributions of cylinders at their steady state conditions at $z = L/2$. For FG and UD-graphene reinforced cylinders under the same conditions, Figures 7a and 7b also illustrate temperature time histories and steady state temperature profiles, respectively. These figures disclose that nanofiller distribution not only affects stationary times but also governs the obtained temperature profiles such that X cylinder has the shortest stationary time and O cylinder has the longest one. Furthermore, it shows that temperature at locations with higher concentration of nanofiller are closer to that of the nearest boundary. Comparison between the effects of graphene and CNT on thermal responses shows

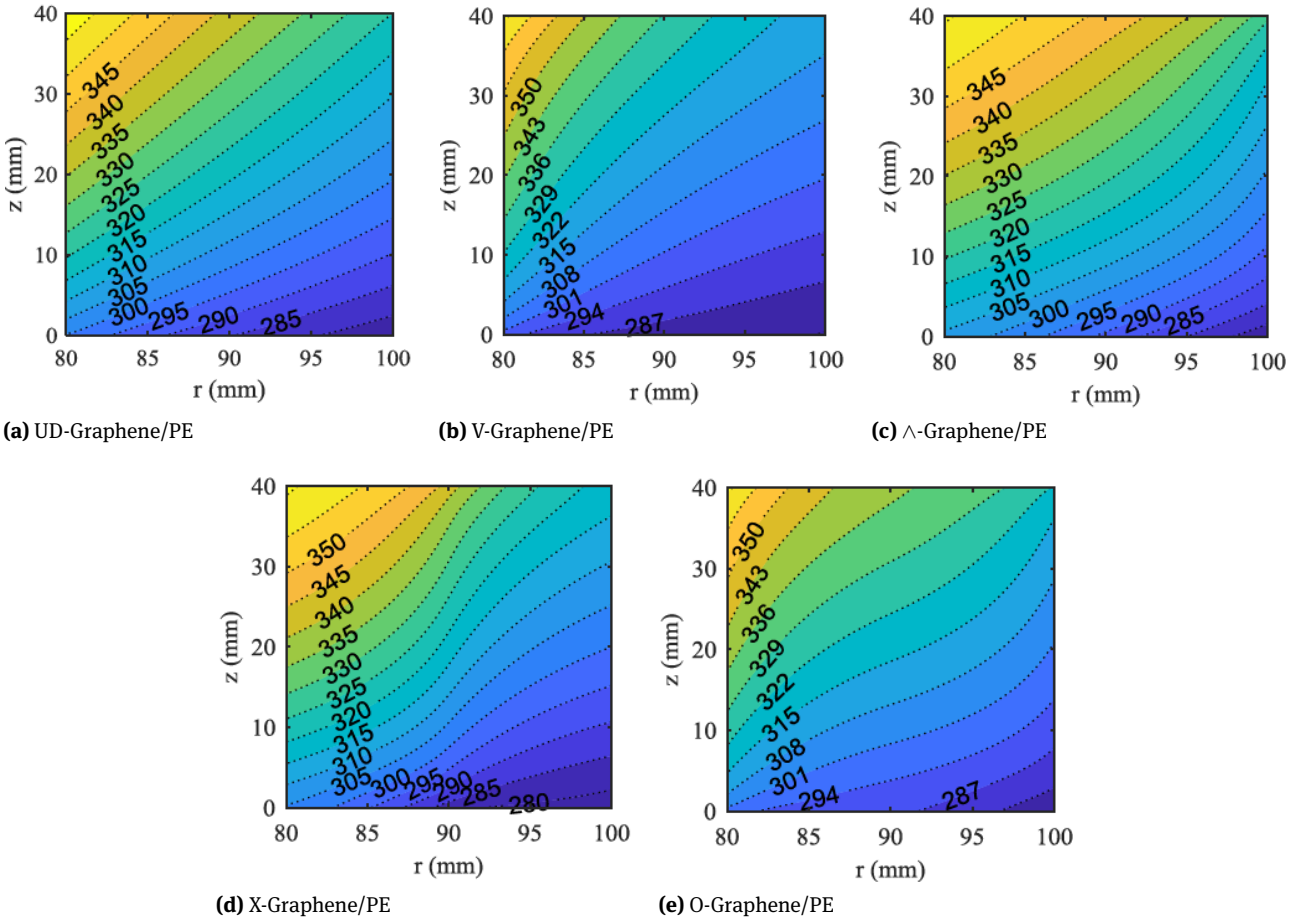

(a) UD-Graphene/PE **(b)** V-Graphene/PE **(c)** ∧-Graphene/PE

(d) X-Graphene/PE **(e)** O-Graphene/PE

Figure 8: Two-dimensional temperature (K) profiles a) UD, b) V, c) ∧, d) X and e) O-graphene/PE cylinders subjected to inner and upper heat fluxes, and outer and lower cold convection environments

that graphene reinforced cylinders have lower temperature variation than those reinforced with CNT because they have higher thermal conductivity as shown in Figure 3. It should be mentioned that cylinders with higher thermal conductivity have a better thermal flow which results in cylinders with lower temperature variation.

Moreover, Figure 8 illustrates the two-dimensional temperature profiles of the considered graphene reinforced cylinders. The significant effect of graphene dispersion on temperature profile are clearly visible in this figure such that the highest temperature is observed in V-type cylinder and it has a smallest high spread at its outer lower part, while ∧-type cylinder has the biggest high temperature spread at its inner upper part.

In order to investigate the effect of nanofiller volume fraction on thermal responses, X-CNT/PE and X-graphene/PE nanocomposite cylinders with the same dimensions, $T^0 = 300$ K, $f_r^{\min} = 0$ and different $f_r^{\max}$ were considered. The thermal boundary conditions of cylinders were assumed to be $T_i = 300$ K, $T_o = 350$ K and upper and lower faces were thermally insulated. Figures 9 and 10 show the thermal responses of CNT and graphene reinforced cylinders, respectively, in terms of temperature time histories and steady state temperature profiles. The results disclose that the increase of nanofiller contents significantly reduces the stationary time of temperature profiles. It also has a remarkable impact on steady state temperature profiles such that the use of more nanofiller increases the temperature gradient of cylinders. Moreover, it was observed that the use of graphene has stronger effects on stationary time than the use of CNT such that graphene/PE, with higher thermal conductivity than CNT/PE (see Figure 3), has shorter approaching time to steady state condition.

Here, the effects of different thermal boundary conditions on the steady state temperature profiles of graphene/PE with the same dimensions, $f_r^{\min} = 0$ and were investigated. Figure 11 shows two-dimensional tem-

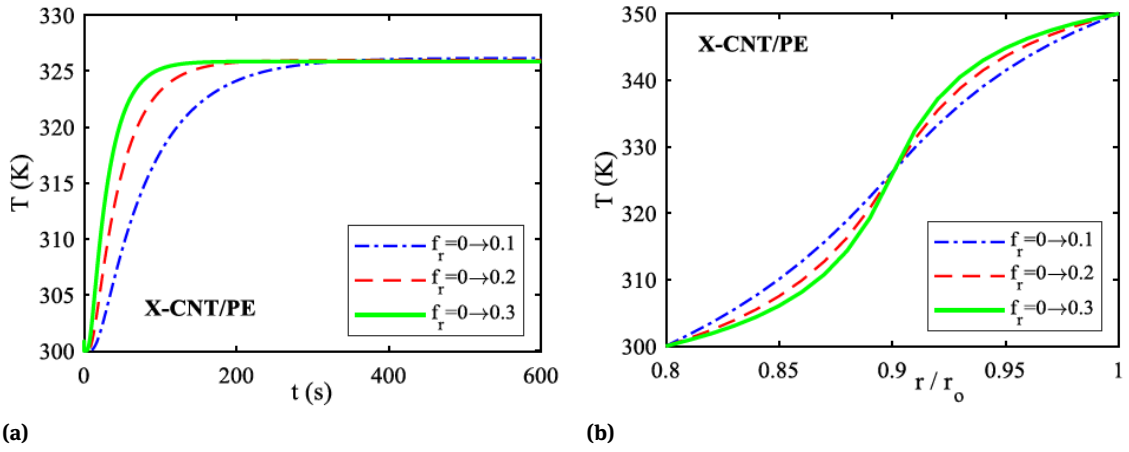

Figure 9: a) Temperature time histories of mid points b) Steady state temperature profiles at in X-CNT/PE cylinders

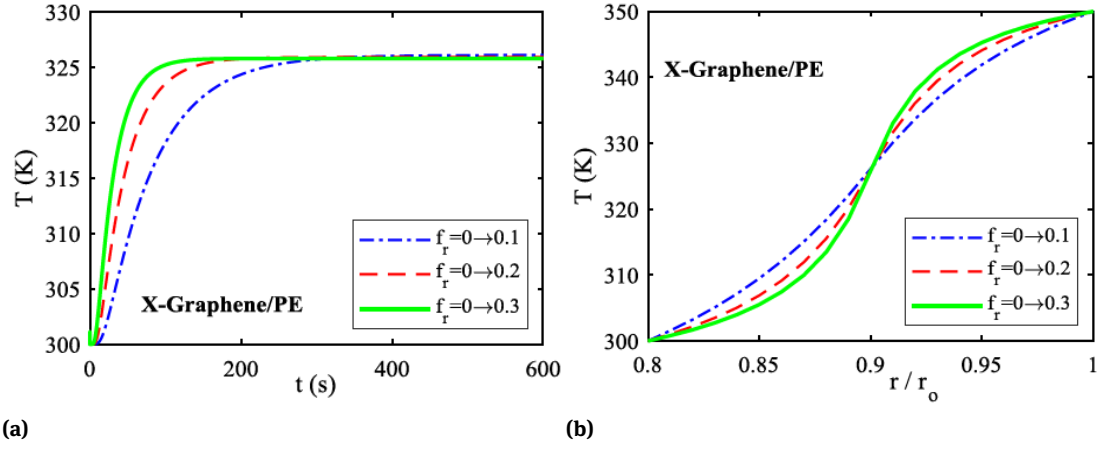

Figure 10: a) Temperature time histories of mid points b) Steady state temperature profiles at $z = L/2$ in X-graphene/PE cylinders

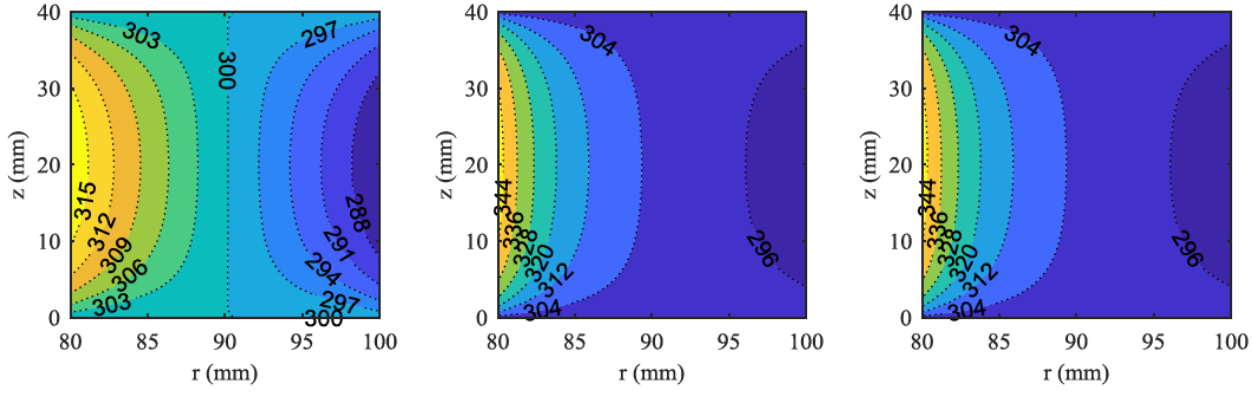

Figure 11: Two-dimensional temperature (K) profiles a) UD, b) V and c) X-graphene/PE cylinders subjected to $Q_i = 5$ kW/m^2 and $Q_o = -Q_i(r_i/r_o)$ and $T_u = T_d = 300$ K

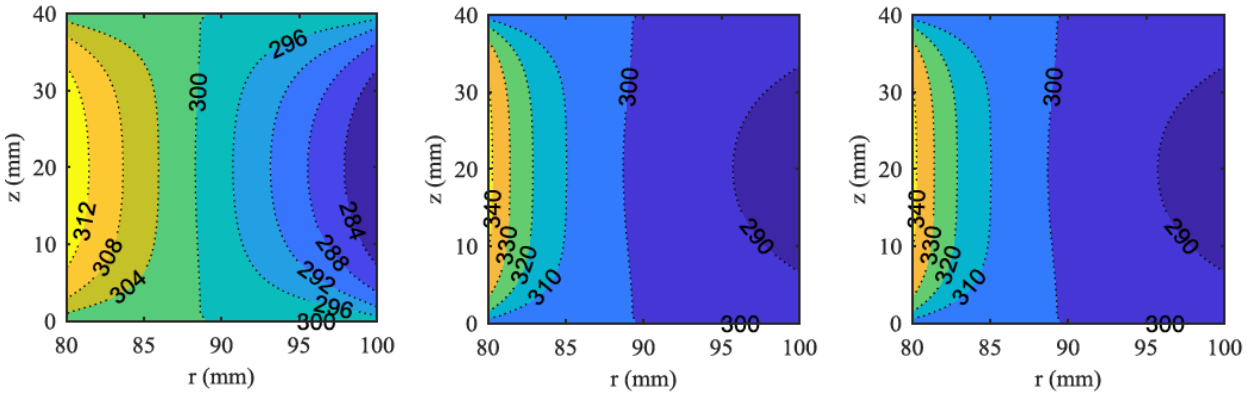

(a) UD-Graphene/PE **(b)** V-Graphene/PE **(c)** X-Graphene/PE

Figure 12: Two-dimensional temperature (K) profiles a) UD, b) V and c) X-graphene/PE cylinders subjected to $Q_i = 5$ kW/m^2, $h_o = 150$ W/(m^{2}K), $T_{a-o} = 250$ K and $T_u = T_d = 300$ K

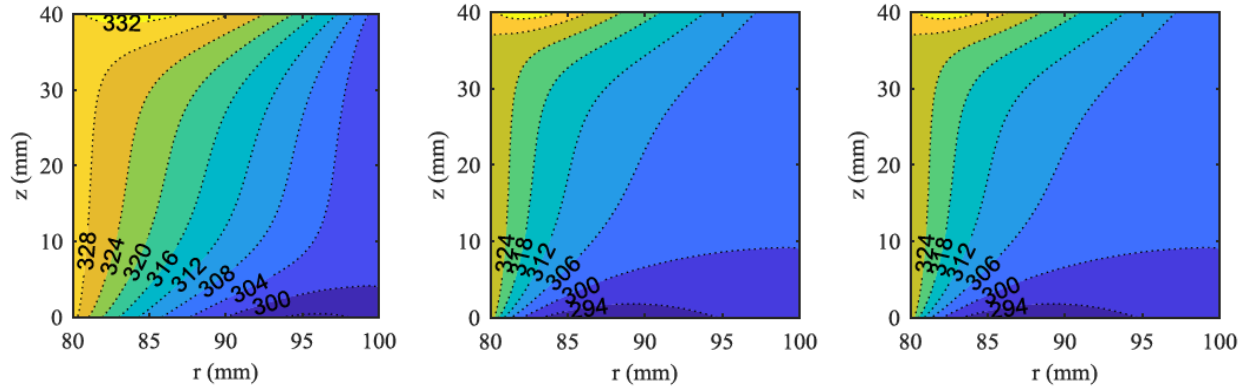

(a) UD-Graphene/PE **(b)** V-Graphene/PE **(c)** X-Graphene/PE

Figure 13: Two-dimensional temperature (K) profiles a) UD, b) V and c) X-graphene/PE cylinders subjected to $T_i = 330$ K, $T_o = 300$ K, $Q_u = 5$ kW/m^2 and $Q_d = -5$ kW/m^2

perature profiles of such cylinders subjected to $Q_i = 5$ kW/m^2, $Q_o = -Q_i(r_i/r_o)$ and $T_u = T_d = 300$ K. Due to symmetric thermal conditions, a symmetric temperature profile was observed for UD and X cylinders although temperature gradient in X cylinder was much higher than UD cylinder. However, V cylinder experiences an asymmetric temperature profile such that the inner half thickness of cylinder has wide temperature gradient and temperature at inner radius goes above 344 K.

Considering an outer thermal convection environment for previous cylinders, Figure 12 illustrates temperature profiles when $h_o = 150$ W/(m^2 K) and $T_{a-o} = 250$ K. The obtained temperature profiles show that the effects of such heat convection environment are higher than employed internal heat flux because coldness (T<300 K) spread is more visible in all figures.

Figure 13 also shows temperature profiles for such cylinders when thermal boundary conditions are $T_i = 330$ K, $T_o = 300$ K, $Q_u = 5$ kW/m^2 and $Q_d = -5$ kW/m^2. Although temperature profiles of UD and X cylinders are almost the same, temperature variation in X cylinder is higher than the other one due to its sharper variation in nanofiller dispersion. In V cylinder, coldness spread is dominant because of the allocation of nanofillers in the outer half thickness of cylinder.

5 Conclusions

In this paper, the impacts of graphene and CNT to steady state and transient heat transfer behaviors of FG nanocomposite axisymmetric cylinders were investigated using a

mesh-free method under different types of thermal boundary conditions. By employing a micromechanical model, the thermal properties of nanocomposite materials were calculated. The effects of nanofiller content and distribution as well as thermal boundary conditions on the heat transfer behaviors of nanocomposite cylinders were studied which resulted in the following main conclusions:

- The use of nanofiller and the increase of its amount result in shorter stationary times such that the increase $f_r^{\max}$ of from 0.1 to 0.3 leads to the reduction of stationary time from 400 s to 100 s.
- The allocation of nanofiller close to the boundaries leads to approaching the temperatures of the nearest boundary.
- The FG allocation of nanofiller intensifies temperature gradient and thermal management of FG nanocomposite cylinders. In one case shown in Figure 6, it was observed that T_i in V-CNT/PE cylinder was around 356 K while in UD and $\wedge$-CNT/PE cylinder T_i =344 K.
- The use of graphene in nanocomposite has stronger impact on thermal response than the use of CNT. Comparing Figure 6b and 7b shows that the use of graphene leads to better conduction such that T_i in graphene/PE cylinders is 10 K less than CNT/PE cylinders.

Acknowledgement: The work described in this paper was supported by National Natural Science Foundation of China (Grant no. 11972204) and Natural Sciences and Engineering Research Council of Canada (NSERC under grant RGPIN-217525). The authors are grateful for their supports.

References

[1] Power A.C., Gorey B., Chandra S., Chapman J., Carbon nanomaterials and their application to electrochemical sensors: A review, Nanotechnol. Rev., 2018, 7, 19-41.

[2] Kalavakunda V., Hosmane N.S., Graphene and its analogues, Nanotechnol. Rev., 2016, 5, 369-376.

[3] Fujii M., Zhang X., Xie H., Ago H., Takahashi K., Ikuta T., Abe H., Shimizu T., Measuring the thermal conductivity of a single carbon nanotube, Phys. Rev. Lett., 2005, 95.

[4] Samani M.K., Khosravian N., Chen G.C.K., Shakerzadeh M., Baillargeat D., Tay B.K., Thermal conductivity of individual multiwalled carbon nanotubes, Int. J. Therm. Sci., 2012, 62, 40-43.

[5] Balandin A.A., Ghosh S., Bao W., Calizo I., Teweldebrhan D., Miao F., Lau C.N., Superior Thermal Conductivity of Single-Layer Graphene, Nano. Lett., 2008, 8, 902-907.

[6] Fattahi A.M., Safaei B., Ahmed N.A., A comparison for the nonclassical plate model based on axial buckling of single-layered graphene sheets, Eur. Phys. J. Plus., 2019; 134, 555.

[7] Safaei B., Fattahi A.M., Chu F., Finite element study on elastic transition in platelet reinforced composites, Microsyst. Technol., 2018, 24, 2663-2671.

[8] Sahmani S., Safaei B., Nonlocal strain gradient nonlinear resonance of bi-directional functionally graded composite micro/nano-beams under periodic soft excitation, Thin-Walled Struct., 2019, 143, 106226.

[9] Ghanati P., Safaei B., Elastic buckling analysis of polygonal thin sheets under compression, Indian J. Phys., 2019, 93, 47-52.

[10] Moradi-Dastjerdi R., Behdinan K., Stability analysis of multifunctional smart sandwich plates with graphene nanocomposite and porous layers, Int. J. Mech. Sci., 2020, 167, 105283.

[11] Huang C., Qian X., Yang R., Thermal conductivity of polymers and polymer nanocomposites, Mater. Sci. Eng. R. Reports, 2018, 132, 1-22.

[12] Gori F., Corasaniti S., Effective thermal conductivity of composites, Heat Mass Transf., 2014, 77, 653-661.

[13] Balandin A.A., Thermal properties of graphene and nanostructured carbon materials, Nat. Mater., 2011, 10, 569-581.

[14] Chung D.D.L., Materials for thermal conduction, Appl. Therm. Eng., 2001, 21, 1593-1605.

[15] Biercuk M.J., Llaguno M.C., Radosavljevic M., Hyun J.K., Johnson A.T., Fischer J.E., Carbon nanotube composites for thermal management, Appl. Phys. Lett., 2002, 80, 2767-2769.

[16] Huxtable S.T., Cahill D.G., Shenogin S., Xue L., Ozisik R., Barone P., et al., Interfacial heat flow in carbon nanotube suspensions, Nat. Mater. 2003, 2, 731-734.

[17] Choi S.U.S., Zhang Z.G., Yu W., Lockwood F.E., Grulke E.A., Anomalous thermal conductivity enhancement in nanotube suspensions, Appl. Phys. Lett. 2001, 79, 2252-2254.

[18] Gu J., Li N., Tian L., Lv Z., Zhang Q., High thermal conductivity graphite nanoplatelet/UHMWPE nanocomposites, R.S.C. Adv., 2015,5, 36334-36339.

[19] Zabihi Z., Araghi H., Effective thermal conductivity of carbon nanostructure based polyethylene nanocomposite: Influence of defected, doped, and hybrid filler, Int. J. Therm. Sci., 2017, 120, 185-189.

[20] Moheimani R., Hasansade M., A closed-form model for estimating the effective thermal conductivities of carbon nanotube-polymer nanocomposites, Proc. Inst. Mech. Eng. Part C J. Mech. Eng. Sci., 2019, 233, 2909-2919.

[21] Qin Z., Zhao S., Pang X., Safaei B., Chu F., A unified solution for vibration analysis of laminated functionally graded shallow shells reinforced by graphene with general boundary conditions, Int. J. Mech. Sci., 2020, 105341.

[22] Qin Z., Pang X., Safaei B., Chu F., Free vibration analysis of rotating functionally graded CNT reinforced composite cylindrical shells with arbitrary boundary conditions, Compos. Struct., 2019, 220, 847-860.

[23] Qin Z., Safaei B., Pang X., Chu F., Traveling wave analysis of rotating functionally graded graphene platelet reinforced nanocomposite cylindrical shells with general boundary conditions, Results Phys., 2019, 15, 102752.

[24] Shokri-Oojghaz R., Moradi-Dastjerdi R., Mohammadi H., Behdinan K., Stress distributions in nanocomposite sandwich cylinders reinforced by aggregated carbon nanotube, Polym. Compos., 2019, 40, E1918-E1927.

[25] Moradi-Dastjerdi R., Payganeh G., Tajdari M., Thermoelastic Analysis of Functionally Graded Cylinders Reinforced by Wavy CNT

Using a Mesh-Free Method, Polym. Compos., 2018, 39, 2190-2201.
[26] Moradi-Dastjerdi R., Payganeh G., Thermoelastic dynamic analysis of wavy carbon nanotube reinforced cylinders under thermal loads, Steel Compos. Struct., 2017, 25, 315-326.
[27] Moradi-Dastjerdi R., Payganeh G., Thermoelastic Vibration Analysis of Functionally Graded Wavy Carbon Nanotube-Reinforced Cylinders, Polym. Compos. 2018, 39, E826-E834.
[28] Safaei B., Ahmed N.A., Fattahi A.M., Free vibration analysis of polyethylene/CNT plates, Eur. Phys. J. Plus., 2019, 134, 271.
[29] Safaei B., Moradi-Dastjerdi R., Behdinan K., Chu F., Critical buckling temperature and force in porous sandwich plates with CNT-reinforced nanocomposite layers, Aerosp. Sci. Technol., 2019, 91, 175-185.
[30] Safaei B., Moradi-Dastjerdi R., Behdinan K., Qin Z., Chu F., Thermoelastic behavior of sandwich plates with porous polymeric core and CNT clusters/polymer nanocomposite layers, Compos. Struct., 2019, 226, 111209.
[31] Damadam M., Moheimani R., Dalir H., Bree's diagram of a functionally graded thick-walled cylinder under thermo-mechanical loading considering nonlinear kinematic hardening, Case Stud. Therm. Eng., 2018, 12, 644-654.
[32] Jalali M.H., Zargar O., Baghani M., Size-Dependent Vibration Analysis of FG Microbeams in Thermal Environment Based on Modified Couple Stress Theory, Iran J. Sci. Technol.- Trans. Mech. Eng., 2019, 43, 761-771.
[33] Pourasghar A., Chen Z., Effect of hyperbolic heat conduction on the linear and nonlinear vibration of CNT reinforced size-dependent functionally graded microbeams, Int. J. Eng. Sci., 2019, 137, 57-72.
[34] Pourasghar A., Zhao C., Hyperbolic heat conduction and thermoelastic solution of functionally graded CNT reinforced cylindrical panel subjected to heat pulse, Int. J. Solids Struct., 2019, 163, 117-129.
[35] Safaei B., Moradi-Dastjerdi R., Qin Z., Behdinan K., Chu F., Determination of thermoelastic stress wave propagation in nanocomposite sandwich plates reinforced by clusters of carbon nanotubes, J. Sandw. Struct. Mater., 2019, DOI: 10.1177/1099636219848828.
[36] Zargar O., Mollaghaee-Roozbahani M., Bashirpour M., Baghani M., The application of Homotopy Analysis Method to determine the thermal response of convective-radiative porous fins with temperature-dependent properties, Int. J. Appl. Mech., 2019, https://doi.org/10.1142/S1758825119500893.
[37] Moradi-Dastjerdi R., Behdinan K., Thermoelastic static and vibrational behaviors of nanocomposite thick cylinders reinforced with graphene, Steel Compos. Struct., 2019, 31, 529-539.
[38] Moradi-Dastjerdi R., Payganeh G., Transient heat transfer analysis of functionally graded CNT reinforced cylinders with various boundary conditions, Steel Compos. Struct., 2017, 24, 359-367.
[39] Deng F., Zheng Q.S., Wang L.F., Nan C.W., Effects of anisotropy, aspect ratio, and nonstraightness of carbon nanotubes on thermal conductivity of carbon nanotube composites, Appl. Phys. Lett. 2007, 90.
[40] Evans W., Prasher R., Fish J., Meakin P., Phelan P., Keblinski P., Effect of aggregation and interfacial thermal resistance on thermal conductivity of nanocomposites and colloidal nanofluids, Int. J. Heat Mass Transf., 2008, 51, 1431-1438.
[41] Haggenmueller R., Guthy C., Lukes J.R., Fischer J.E., Winey K.I., Single wall carbon nanotube/polyethylene nanocomposites: Thermal and electrical conductivity, Macromolecules, 2007, 40, 2417-2421.
[42] Hetnarski R.B., Eslami M.R., Thermal stresses-advanced theory and applications, The Netherlands: Springer; 2009.
[43] Lancaster P., Salkauskas K., Surface Generated by Moving Least Squares Methods, Math. Comput., 1981, 37, 141-158.